Excitation by Scattering/Total Field Decomposition and Uniaxial PML in the Geometric Formulation

Matteo Cicuttin[1], Lorenzo Codecasa[2], Ruben Specogna[1], and Francesco Trevisan[1]

[1]Dipartimento di Ingegneria Elettrica Gestionale e Meccanica, Università di Udine, Udine I-33100, Italy
[2]Dipartimento di Elettronica, Informazione e Bioingegneria, Politecnico di Milano, Milan I-20133, Italy

This paper presents a general technique to apply excitations in the framework of discrete geometric numerical methods using dual grids, such as discrete geometric approach and finite integration technique. The technique overcomes some limitations of the impedance boundary condition we proposed in a previous work, especially when dealing with waveguides, where specific excitation modes must be applied. The proposed approach is based on a scattering/total field decomposition, which, if needed, allows to study scatterings due to objects.

***Index Terms*— Discrete geometric approach (DGA), finite integration technique, modal excitation, port boundary condition, waveguide.**

I. Introduction

In [1], it was shown how a plane wave excitation can be integrated in the framework of the discrete geometric approach (DGA). The purpose was attained using an impedance boundary condition that allowed to simulate the plane wave. This kind of excitation, however, finds limited application in simulating waveguides. In particular, it can only be applied at waveguide ports, where the contributions of high-order modes can be neglected; otherwise, different impedances of the modes will cause reflections. When multiple modes are present, a more general approach is required. A possible technique is to split the domain in a scattering region Ω_s and a total region Ω_t, and to apply the excitation at the interface Σ between these two regions. Reflections due to the domain truncation are avoided by terminating the two regions with uniaxial perfectly matched layers (UPMLs) [2], as depicted in Fig. 1. An advantage of this kind of arrangement is that it allows the presence of objects producing scatterings in the surroundings of the interface Σ. In addition, if only the scattered field or the total field needs to be computed, the parts of Ω_t or Ω_s that are not PML can be omitted without compromising the effectiveness of the method. The excitation is applied on the interface Σ between Ω_s and Ω_t by means of a dual boundary grid [8], [9]. In this paper, it is shown how this technique can be extended to the finite integration technique [4], DGA [3], cell method [5], and other methods involving dual-cell complexes. To this aim, the following discussion will be focused on a piece of rectangular waveguide, but the technique can be applied to guides of an arbitrary shape. In Section II, we provide a brief description of the discrete electromagnetic wave propagation problem. In Section III, we discuss the scattering field/total field decomposition. In particular, we show that Maxwell's equations and constitutive relations must be modified to account for the excitation contribution imposed on Σ. Section IV is devoted to the discussion on how the excitation is actually specified. The results of a couple of numerical experiments are shown in Section V. Finally, the conclusion is drawn in Section VI.

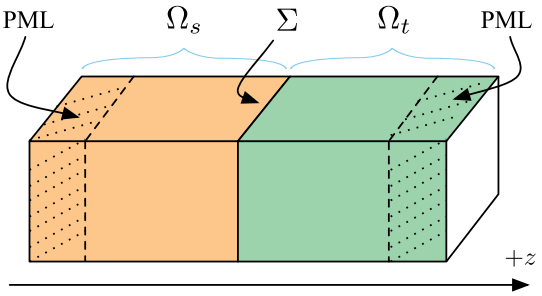

Fig. 1. Subregions of the problem: PMLs, scattered field region Ω_s, and total field region Ω_t. Excitation is applied on the interface Σ.

II. Electromagnetic Wave Propagation in Frequency Domain

The time-harmonic electromagnetic wave propagation in a region of space Ω is described in terms of the usual Maxwell differential formulation [6] as

$$\nabla \times (\boldsymbol{\nu} \nabla \times \boldsymbol{e}) - \omega^2 \boldsymbol{\epsilon} \boldsymbol{e} = \mathbf{0} \tag{1}$$

where $\boldsymbol{\nu}$ and $\boldsymbol{\epsilon}$ are the material tensors, ω is the angular frequency, and $\boldsymbol{e}$ is an unknown complex-valued vector function describing the electric field. The numerical treatment of (1) requires the discretization of Ω, which is obtained by means of a primal tetrahedral grid $\mathcal{G}$ and a dual-grid $\tilde{\mathcal{G}}$ induced by the barycentric subdivision of $\mathcal{G}$. As prescribed by the DGA method, integral quantities are associated to the elements of these interlocked grids, especially the following quantities:

1) electromotive force U_k to edges $e_k \in \mathcal{G}$;
2) magnetic flux Φ_k to faces $f_k \in \mathcal{G}$;
3) magnetomotive force F_k to edges $\tilde{e}_k \in \tilde{\mathcal{G}}$;
4) electric flux Ψ_k to faces $\tilde{f}_k \in \tilde{\mathcal{G}}$.

These quantities are stored in the corresponding arrays $\mathbf{U}$, $\mathbf{\Phi}$, $\mathbf{F}$, and Ψ containing electromotive forces, magnetic fluxes, magnetomotive forces, and electric fluxes for the whole mesh, respectively. By introducing the face-edge incidence matrix $\mathbf{C}$,

Manuscript received July 1, 2015; revised September 3, 2015 and October 9, 2015; accepted October 19, 2015. Date of publication October 26, 2015; date of current version February 17, 2016. Corresponding author: M. Cicuttin (e-mail: matteo.cicuttin@uniud.it).

Color versions of one or more of the figures in this paper are available online at http://ieeexplore.ieee.org.

Digital Object Identifier 10.1109/TMAG.2015.2494062

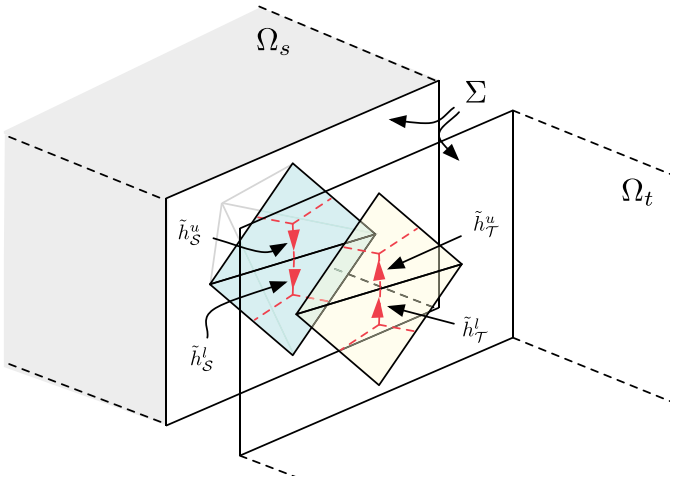

Fig. 2. Boundary primal edges e^{Σ}_k and dual edges $\tilde{e}^{\Sigma}_k$ introduced in the interface between the total field and scattered field regions.

discrete Maxwell's equations can be written; in particular, the discrete Ampère–Maxwell law is written as

$$\mathbf{C}^T\mathbf{F} = i\omega\mathbf{\Psi} \tag{2}$$

while the discrete Faraday–Neumann law as

$$\mathbf{CU} = -i\omega\mathbf{\Phi}. \tag{3}$$

Primal quantities and dual quantities are related by the constitutive relations

$$\mathbf{\Psi} = \mathbf{M}_\epsilon\mathbf{U} \tag{4}$$

$$\mathbf{F} = \mathbf{M}_\nu\mathbf{\Phi} \tag{5}$$

where $\mathbf{M}_\nu$ and $\mathbf{M}_\epsilon$ are the constitutive matrices, which are built as prescribed by the energetic approach for tetrahedra [7]. Some algebraic manipulation of (2)–(5) yields the discrete wave propagation problem in the frequency domain

$$\mathbf{C}^T\mathbf{M}_\nu\mathbf{CU} - \omega^2\mathbf{M}_\epsilon\mathbf{U} = \mathbf{0} \tag{6}$$

which is the discrete counterpart of problem (1).

III. Scattered Field/Total Field Formulation

The electromagnetic field computed in the Ω_t region is the sum of the field due to the excitation imposed on Σ and, if scattering objects are present in Ω_t, the field due to the reflections produced by the scatterer (Fig. 2). On the other hand, the scattering field in the region Ω_s is only due to the reflections occurring in Ω_t returning back to Ω_s. In both the regions, the wave propagation phenomenon occurs as prescribed by (1), but on Σ, a transition from the total field to the scattered field happens. The transition is obtained by adding the excitation contribution on the boundary primal and dual edges on Σ. This is better explained by thinking the scattering field region and the total field region as separated (Fig. 2). In this way, the boundary Σ is split into two parts: 1) a part pertaining to Ω_t and 2) a part pertaining to Ω_s. On the Ω_s side, the electromotive and magnetomotive forces on the edges of Σ can be decomposed in an excitation component and a scattering component. At the same time, the electromagnetic quantities on the Ω_t side of Σ must be constrained to be equal to the ones associated with the corresponding edges of the Ω_s side. This requires the modification of the Ampère–Maxwell law, the Faraday–Neumman law, and the constitutive relations in the volume elements of Ω_s touching Σ as explained in Sections III-A–III-C. In the following, local laws are described (which involve local quantities denoted by the superscript υ), and then it is shown how local laws are used to derive the global problem. For clarity of notation, the superscript υ is omitted from the incidence matrices: when used with local quantities, $\mathbf{C}$ and $\mathbf{C}^T$ are considered to be the local incidence matrices, otherwise they are considered to be the global ones.

A. Ampère–Maxwell Law

The Ampère–Maxwell law involves the edges of the boundary dual grid $\tilde{\mathcal{G}}^{\Sigma}$ on Σ. The boundary dual edges $\tilde{e}^{\Sigma}_{\mathcal{T}}$ and $\tilde{e}^{\Sigma}_{\mathcal{S}}$ are depicted in Fig. 2 as dashed lines. Each edge lies within two tetrahedra, and can be split into half-edges, such that $\tilde{e}^{\Sigma}_{\mathcal{T}} = \tilde{h}^u_{\mathcal{T}} \cup \tilde{h}^l_{\mathcal{T}}$ and $\tilde{e}^{\Sigma}_{\mathcal{S}} = \tilde{h}^u_{\mathcal{S}} \cup \tilde{h}^l_{\mathcal{S}}$ (Fig. 2). Each half-edge belongs to a single tetrahedron; for example, $\tilde{h}^u_{\mathcal{T}}$ belongs to the upper tetrahedron in $\Omega_{\mathcal{T}}$, while $\tilde{h}^l_{\mathcal{S}}$ belongs to the lower tetrahedron in $\Omega_{\mathcal{S}}$ (Fig. 2). The half-edge quantities contribute to the local Ampère–Maxwell law of a single tetrahedron υ.

Considering, for example, the two upper tetrahedra shown in Fig. 2, it can be observed that the magnetomotive forces $F_{\mathcal{T}}$ on $\tilde{h}^u_{\mathcal{T}}$ and $F_{\mathcal{S}}$ on $\tilde{h}^u_{\mathcal{S}}$ must satisfy the relation $F^{\Sigma}_{\mathcal{T}} + F^{\Sigma}_{\mathcal{S}} = 0$, because $\tilde{h}^u_{\mathcal{T}}$ and $\tilde{h}^u_{\mathcal{S}}$ are, in fact, the same edge but with opposite orientation. Moreover, on the Ω_s side, which is where the excitation is applied, the magnetomotive force $F_{\mathcal{S}}$ can be further decomposed in the unknown scattered contribute $F_{\mathcal{S}s}$ and in the known radiated contribute $F_{\mathcal{S}r}$. This implies that the balance of the magnetomotive forces must satisfy the condition $F_{\mathcal{T}} + F_{\mathcal{S}s} = -F_{\mathcal{S}r}$. Thus, the local Ampère–Maxwell law for a tetrahedron υ in $\Omega_{\mathcal{S}}$ touching Σ is written as

$$\mathbf{C}^T\mathbf{F}^{\upsilon} - \mathbf{F}^{\upsilon}_r = i\omega\mathbf{\Psi}^{\upsilon} \tag{7}$$

where the $\mathbf{F}^{\upsilon}$ term collects the circulation of the magnetomotive force in the inner edges of Ω_s, while the $\mathbf{F}^{\upsilon}_r$ term collects the magnetomotive forces on the half-edges of υ due to the excitation.

B. Faraday–Neumann Law

The Faraday–Neumann law involves the primal edges and faces of elements lying on the Ω_s side of Σ. An element can touch Σ with a node, with an edge, or with an entire face. The first case is of no interest, since no nodal quantities are involved in the Faraday–Neumann law, while the second one is only a particularization of the third case. The third case is then analyzed.

Let $f_1, \ldots, f_4$ be the faces of a volume element υ and $\mathbf{\Phi}^{\upsilon} = (\phi^{\upsilon}_1, \ldots, \phi^{\upsilon}_4)$ the array of the magnetic fluxes across them. Without loss of generality, we assume that the face on Σ is f_1, so $\upsilon \cap \Sigma = f_1$. Moreover, also assume that the edges surrounding f_1 are e_1, e_2, and e_3. The electromotive

forces U_1^v, U_2^v, and U_3^v on e_1, e_2, and e_3 and the flux ϕ_1^v on f_1 can be decomposed in an unknown scattering component and in a known radiated component, obtaining $U_k^v = U_{k,s}^v + U_{k,r}^v$ with $k \in \{1, 2, 3\}$ and $\phi_1^v = \phi_{1s}^v + \phi_{1r}^v$. The Faraday–Neumann law can be rewritten as follows:

$$\mathbf{C}\begin{pmatrix} U_{1s}^v + U_{1r}^v \\ U_{2s}^v + U_{2r}^v \\ U_{3s}^v + U_{3r}^v \\ U_4^v \\ U_5^v \\ U_6^v \end{pmatrix} = -i\omega \begin{pmatrix} \phi_{1s}^v + \phi_{1r}^v \\ \phi_2^v \\ \phi_3^v \\ \phi_4^v \end{pmatrix}. \tag{8}$$

By separating known and unknown quantities and writing the equation in a compact form, we obtain

$$\mathbf{C}\big(\mathbf{U}_r^v + \mathbf{U}_s^v\big) = -i\omega\big(\mathbf{\Phi}_r^v + \mathbf{\Phi}_s^v\big). \tag{9}$$

C. Constitutive Relations

A reasoning similar to the one carried out for the Faraday–Neumann law applies for the constitutive relations when writing them for the elements on the Ω_s side touching Σ. Using the setting described in section III-B, electromotive forces are split into scattered and radiated contributions

$$\mathbf{\Psi}^v = \mathbf{M}_\epsilon^v \begin{pmatrix} U_{1s}^v + U_{1r}^v \\ U_{2s}^v + U_{2r}^v \\ U_{3s}^v + U_{3r}^v \\ v U_4^v \\ U_5^v \\ U_6^v \end{pmatrix} = \mathbf{M}_\epsilon^v \begin{pmatrix} U_{1s}^v \\ U_{2s}^v \\ U_{3s}^v \\ U_4^v \\ U_5^v \\ U_6^v \end{pmatrix} + \mathbf{M}_\epsilon^v \begin{pmatrix} U_{1r}^v \\ U_{2r}^v \\ U_{3r}^v \\ 0 \\ 0 \\ 0 \end{pmatrix}. \tag{10}$$

The magnetic constitutive equation, on the other hand, has to be used only when a tetrahedron of the Ω_s side is in contact with Σ by a face, since it involves only face quantities. Again, magnetic fluxes are split into scattered and radiated contributions

$$\mathbf{F}^v = \mathbf{M}_\nu^v \begin{pmatrix} \phi_{1s}^v + \phi_{1r}^v \\ \phi_2^v \\ \phi_3^v \\ \phi_4^v \end{pmatrix} = \mathbf{M}_\nu^v \begin{pmatrix} \phi_{1s}^v \\ \phi_2^v \\ \phi_3^v \\ \phi_4^v \end{pmatrix} + \mathbf{M}_\nu^v \begin{pmatrix} \phi_{1r}^v \\ 0 \\ 0 \\ 0 \end{pmatrix}. \tag{11}$$

Written in a compact form, the two constitutive relations become

$$\mathbf{\Psi}^v = \mathbf{M}_\epsilon^v\big(\mathbf{U}_s^v + \mathbf{U}_r^v\big) \tag{12}$$

$$\mathbf{F}^v = \mathbf{M}_\nu^v\big(\mathbf{\Phi}_s^v + \mathbf{\Phi}_r^v\big). \tag{13}$$

D. Problem Assembly

By considering (7), (9), (12), and (13), solving (7) for the quantity $(\mathbf{\Phi}_r^v + \mathbf{\Phi}_s^v)$, substituting (7), (12), and (13), and rearranging, the expression

$$\mathbf{K}^v\mathbf{U}_s^v = -\mathbf{K}^v\mathbf{U}_r^v - i\omega\mathbf{F}_r^v \tag{14}$$

is obtained, where $\mathbf{K}^v = \mathbf{C}^T\mathbf{M}_\nu^v\mathbf{C} - \omega^2\mathbf{M}_\epsilon^v$. Assembling element by element in the usual way, the equation

$$\mathbf{K}\mathbf{U} = -\mathbf{K}\mathbf{U}_r - i\omega\mathbf{F}_r \tag{15}$$

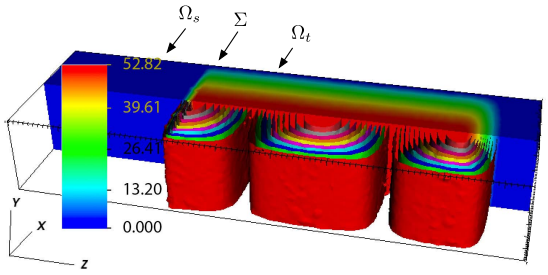

Fig. 3. Waveguide subject of the simulation is depicted, including PMLs, scattering region Ω_s, and total field region Ω_t. The TE_{10} mode excitation is applied on Σ. Dimensions are given in text. Scale: magnitude of the electric field in V/m (solid color region).

is obtained, where all the matrices involved are global. The unknowns $\mathbf{U}_s^v$ from (14) are now part of the unknown $\mathbf{U}$ in (15) and appear in the positions corresponding to the primal edges of Σ. Moreover, the terms $\mathbf{U}_r$ and $\mathbf{F}_r$ are nonzero only in correspondence with the primal edges of Σ and the dual edges of Σ, respectively.

IV. Application of the Excitation on the Interface

At this point, applying the desired excitation is a matter of setting the correct values for the electromotive and magnetomotive forces on both the primal and dual edges of Σ by fixing the values of $U_{k,i}$ and $F_{k,i}$. In the case of the rectangular waveguide of the example, these quantities are calculated by integrating on primal and dual mesh edges, the field computed with the usual closed-form equations for TE and TM modes. Conversely, in the case of an arbitrary shape of the waveguide, the values of $U_{k,i}$ and $F_{k,i}$ are computed by solving a 2-D eigenvalue problem on Σ. We consider Σ planar, but the method can also be applied to curved surfaces by introducing an artificial plane boundary.

V. Numerical Experiments

The presented technique was implemented in EMT, our DGA workbench code written in C++14. The simulations were performed on a Mac OS X 10.9.5 running on a Core i7 3615QM with 16 GB of RAM, a Clang/LLVM 3.5 compiler, and an MKL PARDISO solver. To test the technique, two numerical experiments were prepared. The first one was the simulation of a section of rectangular waveguide (Fig. 3), discretized with a mesh that included 178 280 tetrahedra, yielding a problem of 192 242 unknowns.

Such a toy problem was useful to check the correctness of the results against analytical solutions. In this case, the assembly took 1.84 s, while the solver took 6.44 s. The waveguide dimensions were $a = 60$ mm (in the x-direction) and $b = 30$ mm (in the y-direction), which give a cutoff frequency for the TE_{10} mode of $\sim$2.5 GHz. The length of the PML regions was 30 mm, and the PML regions were implemented according to the UPML technique, as described in [2]. The length of the scattered field region was 30 mm, and the length of the waveguide (total field) region was 100 mm. Finally, the operating frequency was $f = 3.8$ GHz. The computed field configuration was in accordance with an

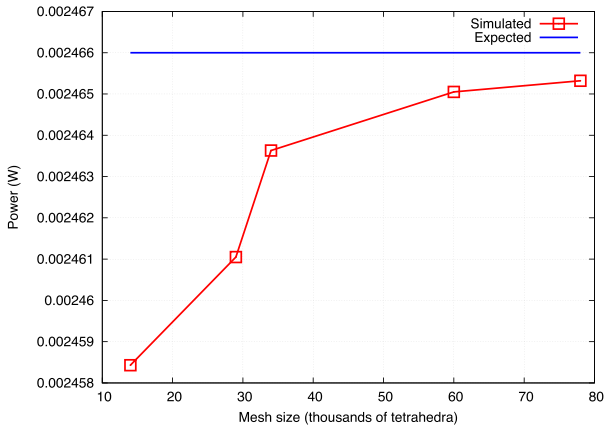

Fig. 4. Problem 1: mesh size (number of tetrahedra) versus power flowing in Ω_t toward positive z. Simulated power is compared with expected theoretical power.

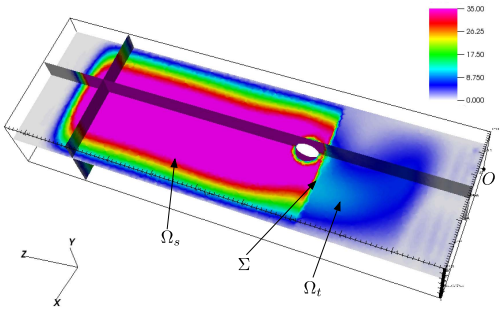

Fig. 5. Scattering field produced in Ω_s by a perfectly conductive sphere of radius $r = 5$ mm, placed off-center ($x = 25$ mm, $y = 20$ mm, $z = 67$ mm, and origin O) near the port.

analytic problem solution. As an additional test, the power flowing in Σ was computed for different mesh sizes (Fig. 4). The flux of the Poynting vector on the interface Σ is computed as [3]

$$P = \frac{1}{2}\mathbf{U}_\Sigma^T \mathbf{F}_\Sigma^* \tag{16}$$

where the arrays $\mathbf{U}_\Sigma$ and $\mathbf{F}_\Sigma$ are, respectively, the electromotive and magnetomotive forces on the edges of Σ.

As a second example, a perfectly conductive sphere of radius $r = 5$ mm was placed inside the waveguide of the previous example, near the port providing the TE_{10} excitation (Fig. 5). In this case, the operating frequency was $f = 4.7$ GHz. The reflections due to the scatterer are visible in the Ω_s region depicted in Fig. 5 together with the transition from the total field to the scattered field.

The proposed approach was validated against a highly accurate in-house developed Finite Element Method (FEM) code (Fig. 6) of the second order and using edge elements. Our approach has the advantage that, unlike FEM, it provides a strong geometrical foundation for the treatment of boundary and interface conditions. The advantage is given by the boundary dual grids (Fig. 2), which allow the manipulation

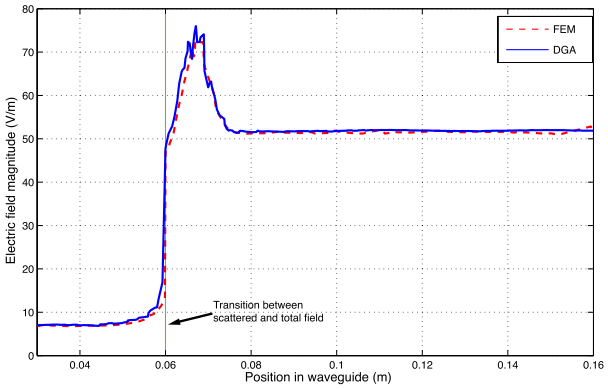

Fig. 6. Problem 2: the technique was compared against an FEM code. The magnitude of the electric field in the scattering and total regions (excluding PML parts) is depicted. The electric field was sampled in the line extending from (0.03, 0.015, 0.03) to (0.03, 0.015, 0.16).

of all quantities related to the boundaries of the simulation domain without using interpolation [1], [3], [8], [9].

VI. Conclusion

A novel technique for the application of excitations on the boundaries of the simulation domain was added to the DGA framework. The technique allows to apply the correct excitations to waveguides, a case where our previous work [1] was of limited applicability. The total/scattered field decomposition, together with the use of PMLs, allowed to overcome the limitations. Moreover, the scattering objects near the scattering/total transition are correctly handled.

Acknowledgment

This work was supported by the Friuli-Venezia Giulia region, Italy, through the PAR FSC 2013 EMCY Project.

References

[1] S. Chialina, M. Cicuttin, L. Codecasa, R. Specogna, and F. Trevisan, "Plane wave excitation for frequency domain electromagnetic problems by means of impedance boundary condition," *IEEE Trans. Magn.*, vol. 51, no. 3, Mar. 2015, Art. ID 7203504.

[2] A. Taflove, *Advances in Computational Electrodynamics*. Norwood, MA, USA: Artech House, 1998.

[3] L. Codecasa, R. Specogna, and F. Trevisan, "Discrete geometric formulation of admittance boundary conditions for frequency domain problems over tetrahedral dual grids," *IEEE Trans. Antennas Propag.*, vol. 60, no. 8, pp. 3998–4002, Aug. 2012.

[4] M. Clemens and T. Weiland, "Discrete electromagnetism with the finite integration technique," *Prog. Electromagn. Res.*, vol. 32, pp. 65–87, 2001.

[5] E. Tonti, "Why starting from differential equations for computational physics?" *J. Comput. Phys.*, vol. 257, pp. 1260–1290, Jan. 2014.

[6] R. E. Collin, *Foundations for Microwave Engineering*, 2nd ed. New York, NY, USA: McGraw-Hill, 1992.

[7] L. Codecasa, R. Specogna, and F. Trevisan, "Symmetric positive-definite constitutive matrices for discrete eddy-current problems," *IEEE Trans. Magn.*, vol. 43, no. 2, pp. 510–515, Feb. 2007.

[8] B. Auchmann and S. Kurz, "The pairing matrix in discrete electromagnetism," *Eur. Phys. J. Appl. Phys.*, vol. 39, no. 2, pp. 133–141, Jun. 2007.

[9] L. Codecasa, "Refoundation of the cell method using augmented dual grids," *IEEE Trans. Magn.*, vol. 50, no. 2, Feb. 2014, Art. ID 7012204.